

# TOP-K MAXIMUM INTENSITY PROJECTION PRIORS FOR 3D LIVER VESSEL SEGMENTATION

Xiaotong Zhang, Alexander Broersen, Gonnie CM van Erp, Silvia L. Pintea, Jouke Dijkstra

Radiology Department, Leiden University Medical Center, Leiden, the Netherlands

## ABSTRACT

Liver-vessel segmentation is an essential task in the pre-operative planning of liver resection. State-of-the-art 2D or 3D convolution-based methods focusing on liver vessel segmentation on 2D CT cross-sectional views, which do not take into account the global liver-vessel topology. To maintain this global vessel topology, we rely on the underlying physics used in the CT reconstruction process, and apply this to liver-vessel segmentation. Concretely, we introduce the concept of *top-k maximum intensity projections*, which mimics the CT reconstruction by replacing the integral along each projection direction, with keeping the top-k maxima along each projection direction. We use these top-k maximum projections to condition a diffusion model and generate 3D liver-vessel trees. We evaluate our 3D liver-vessel segmentation on the 3D-ircadb-01 dataset, and achieve the highest *Dice* coefficient, intersection-over-union (*IoU*), and *Sensitivity* scores compared to prior work.

**Index Terms**— Maximum intensity projection, 3D liver-vessel segmentation, CT segmentation.

## 1. INTRODUCTION

Liver resection is the standard surgical treatment option for primary and secondary liver cancer [1]. In the preoperative planning of the tumor resection, it is essential to minimize perioperative blood loss [1]. Due to the complex anatomy of liver vessels, it is challenging to obtain accurate liver-vessel segmentations automatically.

Liver-vessel segmentation is currently done with convolutional neural networks (CNN). Prior work relies on 2D CNN [2, 3] or 3D CNN [4, 5] methods to perform segmentation on CT images. However, these methods use sub-volumes (cropped in three dimensions) of the CT images. These sub-volumes approaches do not take the global topology of the liver-vessel tree into account which could lead to discontinuous and incomplete vessel tree predictions.

To address these shortcomings, prior work [6, 7, 8] makes use of *maximum intensity projection* (MIP) [9]. Given a 3D volume and a set of directions, MIP computes the maximum voxel value along each direction. Therefore, MIP encodes the global vessel topology on 2D projections, and is charac-

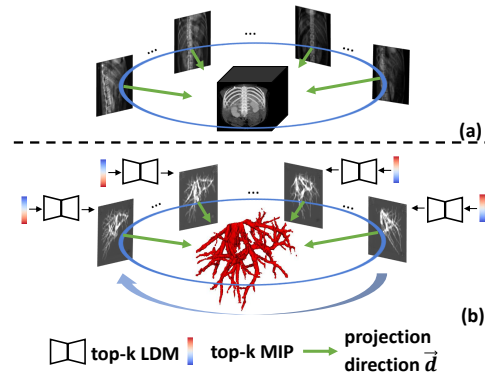


**Fig. 1.** (a) **Standard CT reconstruction:** Given the integral projections and projections directions  $\vec{d}$ , it reconstructs the underlying 3D object by back-projecting the integral along each direction; (b) **Our proposed top-k MIP:** Given the projections directions  $\vec{d}$ , our model reconstructs the 3D liver-vessel tree by computing the top-k maximum value of the CT scan along each direction and inputting this into a latent diffusion model.

terized by high signal-to-noise ratio, while enhancing local vessel probability [9]. However, due to the lack of 3D information, MIP is only an adjunct for segmentation in existing MIP-based methods, which must be combined with a 3D U-Net model [6, 7, 8].

To incorporate the 3D liver-vessel structure, we introduce a *top-k maximum intensity projection (top-k MIP)*. Unlike MIP, which preserves only the maximum voxel value along any given direction, a *top-k MIP* preserves the top-k maximum values along that direction. This allows us to encode fine-grained information regarding the underlying 3D structure of the vessel tree. This information would be missed by simply taking the maximum. Therefore, our model no longer needs to rely on additional 3D convolutions over the CT cross-sectional view to encode this 3D structure.

To sum up, we focus on 3D liver-vessel segmentation by mimicking the process of CT reconstruction [11], as shown in Fig. 1(a). In Fig. 1(b) we propose the *top-k MIP* based 3D vessel segmentation. To reconstruct the 3D liver-vessel tree we use these *top-k MIPs* as conditions in a latent diffusion model (LDM) [10]. Overall, we make the following contributions: (1) we propose incorporating the 3D topology of the liver structure in a principled way by relying on the underlying

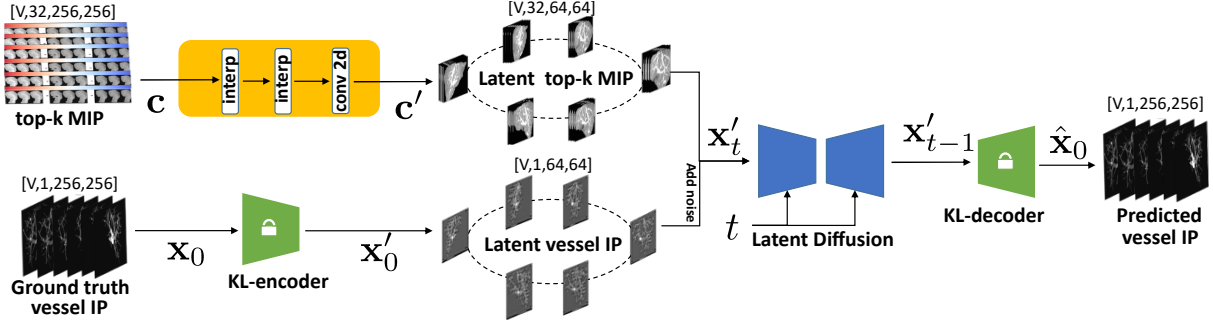


**Fig. 2. Model outline.** Our model represents the global 3D topology of the liver by computing the *top-k MIP* over the CT volume,  $\mathbf{c}$ . Subsequently, it encodes these *top-k MIP* into a latent condition,  $\mathbf{c}'$  (orange). This  $\mathbf{c}'$  latent is used to condition the latent diffusion model (blue) which recovers the ground truth vessel tree  $\mathbf{x}_0$  from noisy inputs  $\mathbf{x}_t$ . We represent the ground truth via *integral projections (IP)* of the 3D ground truth vessel tree. The ground truth  $\mathbf{x}_0$  and the noisy input  $\mathbf{x}_t$  are encoded via a KL-autoencoder (green) to be used in the latent diffusion U-net [10]. We denote the different viewing directions by  $V$  in the batch size.

physics used in CT reconstruction; (2) to this end, we propose a novel *top-k maximum intensity projection* that encodes the fine-grained 3D liver-vessel structure and combine this into a latent diffusion model; (3) finally, we demonstrate improved accuracy of our model on the *3D-ircadb-01* [12] dataset when compared to state-of-the-art methods such *nnUNet* [13], *Swi-nUNetr* [14], *EnsemDiff* [15] and *MedSegDiff* [16].

## 2. TOP-K MAXIMUM INTENSITY PROJECTION FOR LIVER-VESSEL SEGMENTATION

Our model, displayed in Fig. 2, represents the global 3D topological structure of the liver via the *top-k MIP* (denoted by  $\mathbf{c}$ ) of the CT cross-sectional view. We further encode *top-k MIP* (via the yellow block) into the latent condition,  $\mathbf{c}'$ . This  $\mathbf{c}'$  is used to condition the latent diffusion model (depicted in blue) which generates the integral projections of ground truth vessel tree by denoising a given noisy ground truth, in the latent space. The ground truth,  $\mathbf{x}_0$ , and the noisy input  $\mathbf{x}_t$  are represented as *integral projections* over directions  $\vec{d}$  of the true 3D vessel tree segmentation. These *integral projections (IP)* are further encoded/decoded via an autoencoder (depicted in green), to be used in the latent diffusion model.

### 2.1. Ground truth IP and top-k MIP condition

For obtaining the ground truth *integral projection (IP)*, similar to the CT forward projection [11], we assume a bundle of parallel rays  $R^{\vec{d}}$  across different directions  $\vec{d}$ , penetrating the ground truth binary liver-vessel tree, as in Fig. 3(a). The *IP* is the sum of the attenuation coefficient  $\mu$  ( $\mu=1$  for binary liver-vessel trees) along a unit path  $\Delta l^{\vec{d}}$ , which is equivalent to the logarithm of the ratio between the ray intensity  $R^{\vec{d}}$  after the attenuation by the liver vessel tree, and the initial ray

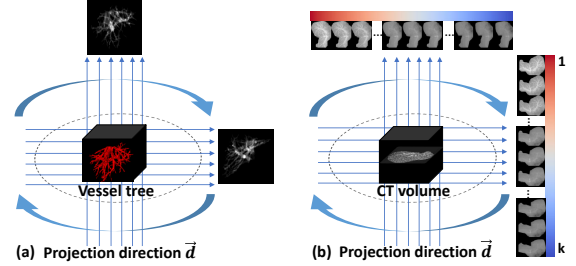


**Fig. 3. (a) Ground truth IP:** We include all vessel tree slices in the *integral projection (IP)* and accumulate them along projection directions  $\vec{d}$ . **(b) Condition top-k MIP:** We include all CT slices in the *top-k maximum intensity projection (top-k MIP)* and keep the *top-k* maxima along projection directions  $\vec{d}$ ;

intensity  $R_0^{\vec{d}}$ :

$$\mathbf{x}_0 \stackrel{\text{def}}{=} \sum_{\Delta l^{\vec{d}}} \mu = -\ln \left( \frac{R^{\vec{d}}}{R_0^{\vec{d}}} \right). \quad (1)$$

For computing the condition  $\mathbf{c}$  to be input to the latent diffusion model we use *top-k MIP*. Different from the integral attenuation in Eq. (1), *top-k MIP* keeps the *top-k* maxima along a ray path  $\Delta l^{\vec{d}}$ , as shown in Fig. 3(b):

$$\mathbf{c} \stackrel{\text{def}}{=} \text{top-}k \left\{ \max \left( \Delta l_i^{\vec{d}} \mu, \Delta l_{i+1}^{\vec{d}} \mu, \dots, \Delta l_n^{\vec{d}} \mu \right) \right\}, \quad (2)$$

where  $n$  is the number of CT voxels located along a ray, and  $\Delta l_i^{\vec{d}} \mu$  is the value of the  $i$ -th CT voxel along the ray.

### 2.2. Top-k MIP conditioning latent diffusion model

We rely on a latent diffusion model [10] conditioned on the *top-k MIP*,  $\mathbf{c}$ , for recovering the denoised liver vessel IPs,  $\hat{\mathbf{x}}_0$ . We encode  $\mathbf{c}$  into a latent vector via interpolation and convolution (yellow block in Fig. 2), into  $\mathbf{c}'$ . Following [10],

we also encode the  $IP$ ,  $\mathbf{x}_0$ , via a pre-trained Kullback-Leibler (KL)-divergence auto-encoder (green blocks in Fig. 2) to obtain  $\mathbf{x}'_0$ .

Standard in the diffusion forward process, we iteratively add Gaussian noise  $\epsilon \sim \mathcal{N}(\mathbf{0}, \mathbf{I})$  to  $\mathbf{x}'_0$ . We aim to denoise the noisy inputs  $\mathbf{x}'_t$ , for  $t \in \{T, \dots, 0\}$  by estimating the noise  $\epsilon_\theta$ , modelled as a U-Net [10] (depicted in blue in Fig. 2). For this, we optimize the parameters of the model,  $\theta$ , by minimizing the loss over time steps,  $t$ :

$$\mathcal{L}_t(\mathbf{x}'_0, \epsilon, \theta) = \|\epsilon_\theta(\mathbf{x}'_t | \mathbf{c}', t) - \epsilon\|_2^2. \quad (3)$$

Once the model is trained, given the encoded  $top-k$  MIP condition  $\mathbf{c}'$ , and the input Gaussian noise  $\mathbf{x}'_T$ , we gradually denoise the noisy input  $\mathbf{x}'_t$ ,  $t \in \{T, \dots, 0\}$  to the estimate of the encoded  $IP$ ,  $\hat{\mathbf{x}}'_0$ . Given the estimate of the encoded  $IP$ ,  $\hat{\mathbf{x}}'_0$ , we decode this via the pre-trained KL-divergence auto-encoder (green block in Fig. 2) into an estimate of the  $IP$ ,  $\hat{\mathbf{x}}_0$ .

### 2.3. Post-processing for artifact suppression

Given the estimated  $IP$ s of the vessel tree,  $\hat{\mathbf{x}}_0$ , we reconstruct the 3D liver vessel tree via filtered back projection (FBP) [11]. Given that, minor inconsistency in the projection domain can cause severe stripe artifacts in the reconstructed images, we employ a simple optimization to suppress these artifacts. Specifically, assume  $\mathbf{T}$  initialized by CT image is a reconstructed liver vessel tree without artifact, and given a matrix  $\mathbf{A}^{\vec{d}}$  recording the voxel indices penetrated by rays under different projection directions  $\vec{d}$ , we impose a projection consistency. Concretely, to dilute the irrelevant background introduced by the initialization of  $\mathbf{T}$ , we enforce that the projection of the reconstructed tree  $\mathbf{T}$  on a certain projection direction encoded in  $\mathbf{A}^{\vec{d}}$  should be as close as possible to the estimated  $IP$  under that projection direction,  $\hat{\mathbf{x}}_0^{\vec{d}}$ :

$$\mathbf{T} = \arg \min_{\mathbf{T}} \sum_{\vec{d}} \|\mathbf{A}^{\vec{d}} \mathbf{T} - \hat{\mathbf{x}}_0^{\vec{d}}\|_2^2. \quad (4)$$

In practice, performing this optimization 10 times is sufficient to suppress the stripe artifacts. Thus, we obtain the binary liver-vessel tree  $\mathbf{T} \geq \text{percentile}(\mathbf{T}, 95)$ . Finally, we perform connected region analysis to cancel small spurious predictions surrounding the segmented vessel tree.

## 3. EXPERIMENTAL EVALUATION

### 3.1. Experimental setting

We evaluate our proposed model on the *3D-ircadb-01* [12] dataset, consisting of 20 CT scans. We exclude the vena cava from the region of interest, using liver masks to focus only the vessels within the liver. We resize the liver-masked ROIs to  $[256 \times 256 \times 256]$  for each CT scan, and project 180 viewing

directions from 0 to 180 degrees for each CT scan, totaling 3600 projections.  $k$  is 32 when creating the  $top-k$  MIP.

Small liver vessel annotations are incomplete in the *3D-ircadb-01* dataset [5]. To mitigate this, we asked clinical experts to score the completeness of the annotations based on a 5-point criterion and picked cases (4, 6, 8, 11, 16) whose score  $\geq 4$  as the test set. We apply leave-one-out cross-validation, such that we have 19 cases (*i.e.* 3420 projections) for training and a single case (*i.e.* 180 projections) for testing, per fold.

We trained *nnUNet*[13] and *SwinUNetr*[14] using 3D CT sub-volumes as input, and using their default pre- and post-processing. For *MedSegDiff*[16] and *EnsemDiff*[15] we used 2D CT slices, and ensemble segmentation results 5 times. Our method does not require an ensemble. For all the experiments, we used an NVIDIA A100 (40GB) GPU.

### 3.2. Experimental results

We report voxel-wise Dice coefficient (*DSC*), Intersection-Over-Union (*IoU*), Sensitivity (*Sen*), Specificity (*Spe*) and centerline Dice coefficient (*clDice*) [17]. Table 1 shows the quantitative evaluation, while Fig. 4 shows a few prediction examples. Our method achieves the highest *DSC*, *IoU*, and *Sen* scores compared to the other baselines on the *3D-ircadb-01* dataset, demonstrating the added value of the proposed top-k MIP projections. *nnUNet* has a higher *clDice* score than our method. However, the vessel centerline was estimated from ground truth vessel annotations, following [17]. Therefore, incomplete and discontinuous voxel-wise ground truth could bias the centerline extraction in *clDice* [17]. Fig. 4 shows that both our method and *nnUNet* predict well-connected vessel structures compared to the ground truth, indicating that *clDice* might not be a sensible choice when comparing segments with inconsistent connectivity. Additionally, all methods in Table 1 have *Spe* scores close to 1, indicating that there are few false positives in liver vessel segmentation.

## 4. DISCUSSION AND LIMITATIONS

**Effect of artifact suppression.** Our model generates liver vessel  $IP$ s based on the intensity of the  $top-k$  MIP. However, due to memory constraints, our current design limits the model from learning correlations between different projection directions. The optimization in Eq. (4) compensates for this shortcoming. This optimization suppresses the reconstruction artifact caused by projection inconsistency.

Table 2 tests the added value of this artifact suppression optimization. The  $IP$ s of the reconstructed vessel tree with artifact suppression have higher *PSNR* [18] and *SSIM* [18], indicating that the optimized  $IP$ s have a similar appearance to the ground truth. Full-view projections in Fig. 5(c)-(d) also show that the vessel  $IP$ s consistency between projections is improved by the artifact suppression.

**Table 1. Quantitative evaluation on the 3D-ircadb-01 [12] dataset.** Our method predicts complete liver-vessel segmentations, while having the highest *IoU*, *Sen* and *DSC* scores. The lower *clDice* scores of our method compared to *nnUNet* could be due to imprecise annotations. Finally, there is a trade-off between complete segmentation (higher *Sen*) or accurate segmentation (higher *Spe*).

	Conv type	View type	<i>DSC</i> (%)	<i>clDice</i> (%)	<i>IoU</i> (%)	<i>Sen</i> (%)	<i>Spe</i> (%)	<i>FLOPs</i> (G)	<i>Params</i> (M)
nnUNet[13]	3D	cross section	58.76 ± 9.89	<b>71.46</b> ± 5.67	42.31 ± 10.19	43.32 ± 11.18	<b>100</b> ± 0	2.90 × 10 <sup>3</sup>	30.7
Swin UNETR[14]	3D	cross section	57.80 ± 9.93	64.16 ± 7.10	41.31 ± 9.51	46.71 ± 13.21	99.96 ± 0.02	6.15 × 10 <sup>2</sup>	62.2
EnsemDiff[15]	2D	cross section	54.82 ± 9.64	60.61 ± 9.55	38.37 ± 9.21	40.05 ± 10.45	99.98 ± 0.02	9.96 × 10 <sup>2</sup>	113.7
MedSegDiff[16]	2D	cross section	59.59 ± 7.73	66.03 ± 8.05	42.85 ± 7.53	47.38 ± 10.44	99.95 ± 0.05	1.05 × 10 <sup>3</sup>	136.8
Ours	2D	projection	<b>64.25</b> ± 7.19	65.87 ± 8.16	<b>47.75</b> ± 8.00	<b>54.03</b> ± 11.23	99.96 ± 0.01	6.83 × 10 <sup>2</sup>	84.5

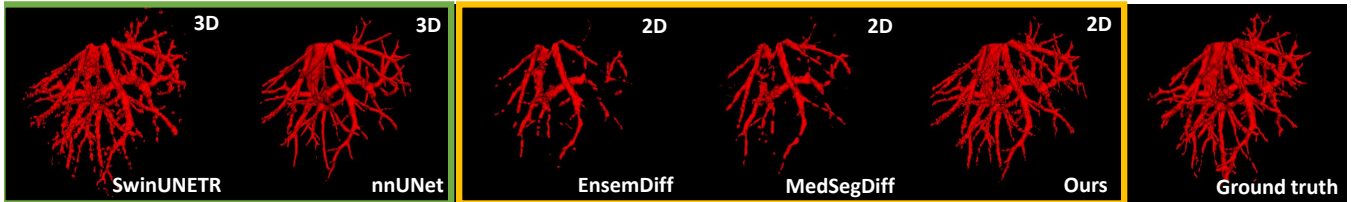


**Fig. 4. Qualitative comparison on the 3D-ircadb-01[12] dataset.** We highlight in green the predictions of the 3D methods and in yellow the predictions of the 2D methods. Our model makes more complete and continuous predictions, resembling the ground truth.

**Table 2. Liver vessel IPs estimation with (w/) and without (w/o) artifact suppression (opt).** Artifact suppression makes the vessel IPs more similar to the ground truth vessel IPs.

	PSNR(↑)	SSIM(↑)
w/o opt	13.51 ± 0.78	0.45 ± 0.07
w/ opt	<b>15.15</b> ± 1.32	<b>0.66</b> ± 0.05

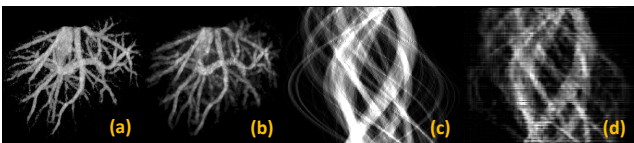


**Fig. 5. Vessel reconstruction with/without artifacts suppression.** (a) reconstructed vessel tree with artifact suppression; (b) reconstructed vessel tree without artifact suppression; (c) full-view projection of a slice of the reconstructed vessel trees with artifacts suppression; (d) full-view projection without artifacts suppression. Artifact suppression improves the consistency between different projection views. The vertical axis in (c) and (d) is the projection view.

**Model limitations.** Our proposed model can handle most cases, where the contrast is within normal ranges, in the liver vessel area. However, segmenting extremely low-contrast vascular regions, as shown in the yellow box in Fig. 6 remains challenging for our model.

**Possible improvements.** Strengthening the correlation between projection views and learning a dynamic projection for the *top-k* MIP are the two improvement directions. Currently, each view is processed independently, and thus we cannot test using the standard MIP. In the standard MIP the depth information is collapsed to a single maximum value, and cannot

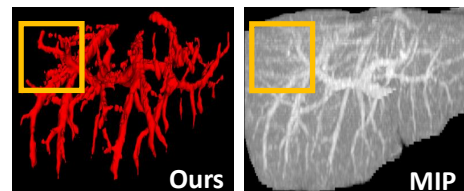


**Fig. 6. Failure analysis.** Correctly segmenting low-contrast CT images is challenging for our method.

be recovered. A model that considers the correlation between projection views, will make it possible to use of the standard MIP, instead of the *top-k* MIP.

## 5. CONCLUSION

We propose a principled way of incorporating 3D liver-vessel topology in 2D diffusion models for liver-vessel segmentation. Accordingly, we draw inspiration from the physics involved in the 3D CT reconstruction. Concretely, we propose to condition a latent diffusion model on *top-k maximum intensity projections* of the CT cross-sectional view. Our proposed model achieves competitive results compared to the existing baselines, validating our approach.

## 6. COMPLIANCE WITH ETHICAL STANDARDS

This research study was conducted retrospectively using human subject data made available in open access by IRCAD, Strasbourg, France. Ethical approval was not required as confirmed by the license attached with the open access data.

## 7. ACKNOWLEDGEMENTS

This work was supported by China Scholarship Council under Grant 202108310010.

## 8. REFERENCES

- [1] O.I. Alirr and A.A.A Rahni, "Survey on liver tumour resection planning system: steps, techniques, and parameters," *Journal of Digital Imaging*, vol. 33, no. 2, pp. 304–323, 2020.
- [2] T. Kitrungrotsakul, X. Han, Y. Iwamoto, L. Lin, A.H. Foruzan, W. Xiong, and Y. Chen, "Vesselnet: A deep convolutional neural network with multi pathways for robust hepatic vessel segmentation," *Computerized Medical Imaging and Graphics*, vol. 75, pp. 74–83, 2019.
- [3] Z. Gao, Q. Zong, Y. Wang, Y. Yan, Y. Wang, N. Zhu, J. Zhang, Y. Wang, and L. Zhao, "Laplacian saliencelated feature pyramid network for accurate liver vessel segmentation," *IEEE Transactions on Medical Imaging*, vol. 42, no. 10, pp. 3059–3068, 2023.
- [4] Q. Huang, J. Sun, H. Ding, X. Wang, and G. Wang, "Robust liver vessel extraction using 3d u-net with variant dice loss function," *Computers in biology and medicine*, vol. 101, pp. 153–162, 2018.
- [5] Q. Yan, B. Wang, W. Zhang, C. Luo, W. Xu, Z. Xu, Y. Zhang, Q. Shi, L. Zhang, and Z. You, "Attention-guided deep neural network with multi-scale feature fusion for liver vessel segmentation," *IEEE Journal of Biomedical and Health Informatics*, vol. 25, no. 7, pp. 2629–2642, 2020.
- [6] Z. Guo, Z. Tan, J. Feng, and J. Zhou, "3d vascular segmentation supervised by 2d annotation of maximum intensity projection," *IEEE Transactions on Medical Imaging*, 2024.
- [7] Y. Liu, H. Kwak, and I. Oh, "Cerebrovascular segmentation model based on spatial attention-guided 3d inception u-net with multi-directional mips," *Applied Sciences*, vol. 12, no. 5, pp. 2288, 2022.
- [8] H. Chen, X. Wang, H. Li, and L. Wang, "3d vessel segmentation with limited guidance of 2d structure-agnostic vessel annotations," *IEEE Journal of Biomedical and Health Informatics*, 2024.
- [9] S. Napel, M.P. Marks, G.D. Rubin, M.D. Dake, C.H. McDonnell, S.M. Song, D.R. Enzmann, and J.R. Jeffrey, "CT angiography with spiral CT and maximum intensity projection," *Radiology*, vol. 185, no. 2, pp. 607–610, 1992.
- [10] R. Rombach, A. Blattmann, D. Lorenz, P. Esser, and B. Ommer, "High-resolution image synthesis with latent diffusion models," in *Proceedings of the IEEE/CVF conference on computer vision and pattern recognition*, 2022, pp. 10684–10695.
- [11] R. Schofield, L. King, U. Tayal, I. Castellano, J. Stirrup, F. Pontana, J. Earls, and E. Nicol, "Image reconstruction: Part 1—understanding filtered back projection, noise and image acquisition," *Journal of cardiovascular computed tomography*, vol. 14, no. 3, pp. 219–225, 2020.
- [12] L. Soler, A. Hostettler, V. Agnus, A. Charnoz, J. Fasquel, J. Moreau, A. Osswald, M. Bouhadjar, and J. Marescaux, "3d image reconstruction for comparison of algorithm database: A patient specific anatomical and medical image database," .
- [13] F. Isensee, P. F. Jaeger, S. A. Kohl, J. Petersen, and K. H. Maier-Hein, "nnu-net: A self-configuring method for deep learning-based biomedical image segmentation," *Nature methods*, vol. 18, no. 2, pp. 203–211, 2021.
- [14] A. Hatamizadeh, V. Nath, Y. Tang, D. Yang, H.R. Roth, and D. Xu, "Swin unetr: Swin transformers for semantic segmentation of brain tumors in mri images," in *International MICCAI Brainlesion Workshop*, September 2021, pp. 272–284.
- [15] J. Wolleb, R. Sandkühler, F. Bieder, P. Valmaggia, and P.C. Cattin, "Diffusion models for implicit image segmentation ensembles," in *International Conference on Medical Imaging with Deep Learning*. December 2022, pp. 1336–1348, PMLR.
- [16] J. Wu, R. FU, H. Fang, Y. Zhang, Y. Yang, H. Xiong, H. Liu, and Y. Xu, "Medsegdiff: Medical image segmentation with diffusion probabilistic model," in *Medical Imaging with Deep Learning*, 2023.
- [17] S. Shit, J.C. Paetzold, A. Sekuboyina, I. Ezhov, A. Unger, A. Zhyhka, J.P.W. Pluim, U. Bauer, and B.H. Menze, "cldice-a novel topology-preserving loss function for tubular structure segmentation," in *Proceedings of the IEEE/CVF conference on computer vision and pattern recognition*, 2021, pp. 16560–16569.
- [18] A. Hore and D. Ziou, "Image quality metrics: Psnr vs. ssim," in *2010 20th international conference on pattern recognition*. IEEE, 2010, pp. 2366–2369.